quaternary

MDPI

Article

Submergence of the Western Greco-Roman Archaeological Site at the Eastern Harbor of Alexandria: Emerged from High Resolution Geophysical Mapping

Amr Hamouda [1], Nader El-Gendy [2], Ahmed El-Shishtawy [2], Suzan El-Gharabawy [1] and Ahmed Fekry [1,*]

[1] Marine Geophysics Lab, National Institute of Oceanography and Fisheries, Alexandria 21556, Egypt; amreu@yahoo.com (A.H.); suzymooo@yahoo.com (S.E.-G.)
[2] Geology Department, Faculty of Science, Tanta University, Tanta 31527, Egypt; naderelgendytanta@yahoo.com (N.E.-G.); am.shishtt@yahoo.com (A.E.-S.)
* Correspondence: fekry@ymail.com

Abstract: Marine geophysical surveys were carried out at the underwater site in the south-western sector of the Eastern Harbor of Alexandria, opposite to the Egyptian Sea Scout Club. Survey works aimed to detect and study the surface and subsurface geomorphological changes caused by historic sea-level rise and natural hazards, by integrating the results of high-resolution geophysical mapping for the seafloor textures and the subsurface layers with previously published core data and sea-level records, the survey works employed echo-sounder, side scan sonar, and sub-bottom profiler. Acoustic data were ground-truthed using an ROV camera and sediment grab sampler. Results of bathymetric mapping and sonar imaging outlined two breakwaters and quay corresponding to a submerged ancient port; also, sediment types were classified according to variation in the magnitude of the backscattered intensities. Interpretation of sub-bottom profiles illustrated the depositional sequence of the topmost sedimentary layers where the sediment thicknesses were thickened by rates that perfectly matched with the recorded sea-level rise rate during the last two millennia, as indicated by isopach maps. Anthropogenic activities were noticed in particular outcropping areas on the sub-bottom profiles. The results explained the role of natural hazards and sea-level rise in changing the geomorphology of the coastline and seabed features.

Keywords: marine geophysical survey; bathymetric mapping; side scan sonar; sub-bottom profiler; acoustic backscatter; seismic interpretation; natural hazards

Citation: Hamouda, A.; El-Gendy, N.; El-Shishtawy, A.; El-Gharabawy, S.; Fekry, A. Submergence of the Western Greco-Roman Archaeological Site at the Eastern Harbor of Alexandria: Emerged from High Resolution Geophysical Mapping. *Quaternary* **2021**, *4*, 22. https://doi.org/10.3390/quat4030022

Academic Editors: Jef Vandenberghe and Leszek Marks

Received: 25 May 2021
Accepted: 20 July 2021
Published: 23 July 2021

1. Introduction

Underwater investigations in the Eastern Harbor of Alexandria (Figure 1) during the last decades have revealed great archaeological findings related to human settlements since the Greek, Roman, and Arabic periods. Among these discoveries are the eastern-side submerged royal quarter including the Emporium, the Poseidium, the Timonitun, the island of Antirrhodus, and the royal palace of Cleopatra, in addition to several port structures and jetties that were recognized in the form of well-founded breakwaters and peers that divide the harbor into several basins [1–4]. Another landmark found was a Roman shipwreck located at the bottom of the harbor near Antirhodus Island [1]. The Eastern Harbor of Alexandria was initiated amid two carbonate ridges since Pleistocene, then sediment loads were transported from the Egyptian offshore shelf and deposited in the harbor basin during transgression of the sea [5]. The recent oval shape of the harbor was formed after being sheltered from the open sea for 3000 years BP, followed by the construction of ancient Alexandria and the royal ports during the Ptolemaic rule (Late Holocene) over a limestone ridge of the Pleistocene age [1,6].

Figure 1. (**a**) Map of the study area in front of Egyptian Sea Scout Club; (**b**) map of the northern part of Egypt; (**c**) map of the Eastern harbor of Alexandria showing the previously detected structures, represented by the light green polygons (after Goddio et al., 1998 [1]); core samples locations are marked by yellow circles (after Stanley et al., 2007 [7]).

The marine survey works extended in the south-western sector of the Eastern Harbor of Alexandria opposite to the Egyptian Sea Scout Club (Figure 1), which lies 20 km west of the north-western Egyptian coastal margin of the Nile Delta. The study area is considered as an underwater heritage site that lies west of the submerged ancient royal port remains, where various Eastern-Mediterranean commercial ports were linked to these ancient ports during the Greek and Roman period [1,3]. Therefore, the city became a capital of significant political value and was a center for international trade between East and West [8]. Previous geoarchaeological investigations indicated that the whole area suffered from several collapses during the last 2000 years [9–12]. The sea-level rise can cause significant changes in coastal zones which leads to the submergence of historic settlements and landscapes [13]. The area of the Eastern harbor of Alexandria was affected by a 2 m post-glacial sea-level rise during the past two millennia [14,15]. The rapid submergence of the structures indicated land subsidence as a result of sediment failure and substrate destabilization [12,16]. Also,

the 365 A.D. tsunami and the following tectonic activities catastrophically affected the ancient coast of Alexandria [11,17]. Submergence was also caused by the overloading of old structures due to insufficient foundation piling over a less compacted base which in turn led to the collapse of these ancient constructions [18,19], where considerable coastal changes can be recorded as a result of human impacts [20].

The main objective of this work was to perform highly detailed geophysical mapping of the submerged site and investigate the seafloor textures and structural features, aiming to study the geomorphological changes resulted from the historic sea-level rise and natural hazards, using an integration of a single beam echo-sounder, side scan sonar, sub-bottom profiler, and ROV video camera.

The bathymetric survey was applied for mapping the seafloor topography and determining the borders of possible archaeological sites [21,22]. A side scan sonar survey was carried out to provide clear images for the seabed textures and detect the exposed archaeological artifacts on the seafloor [23–25]. A seismic profiling survey has been used to trace the subsurface discontinuities, detect the semi-buried archaeological relics, also to study the changes of the coastal geomorphology [26–28], ROV video camera and grab sampler have been used for ground-truthing.

2. Materials and Methods

Marine geophysical surveys were conducted in the south-western sector of the Eastern Harbor opposite to the Egyptian Sea Scout Club (Figure 1a) using a single beam echo-sounder, side scan sonar, and chirp sub-bottom profiler, acoustic data were ground-truthed by ROV video camera and surface sediment samples, while position information was provided by a differential GPS and specialized marine navigational software. Survey grids were limited by particular shallow areas close to the shore (Figure 2).

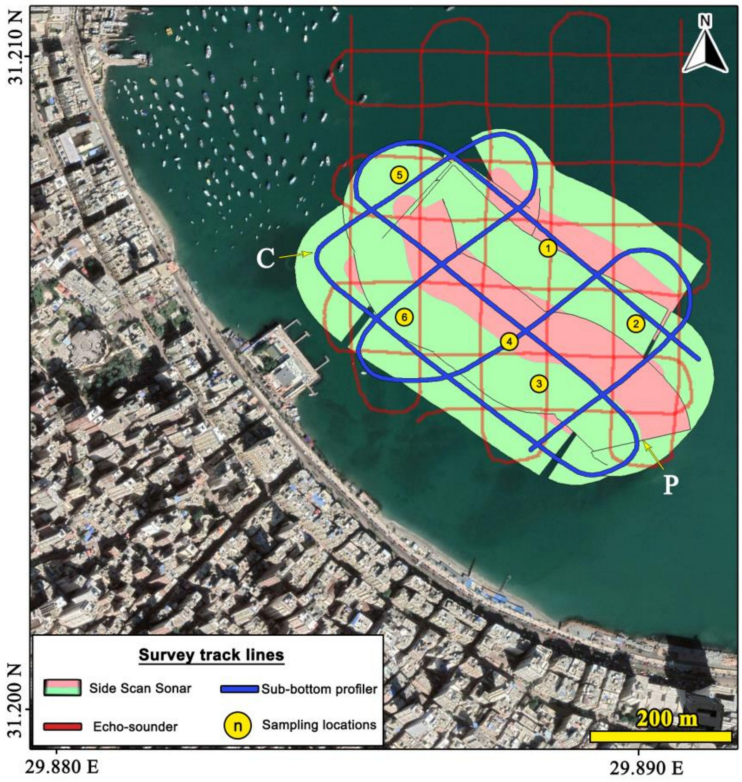

Figure 2. Map of the survey track lines in the study area.

The bathymetric survey was run out using a dual-frequency echo-sounder (Teledyne Odom-Echotrac MK III), the transducer was pole-mounted to the port side of the survey vessel 0.5 m below the sea surface and provided 0.01 m resolution, survey grid consisted

of thirteen survey lines that spaced 100 m from each other in both headings (Figure 2), bathymetric data close to the southern and south-western coast could not be acquired due to the extremely shallow water depths, the corresponding depth values were digitized from previous survey works [1] and grided with the acquired thirteen lines, constructing bathymetric contour map using Surfer software.

Sonar imaging survey was carried out using Edge-Tech 4200 side scan sonar (SSS), which provides high resolution sonar images for the seafloor by operating dual simultaneous frequencies at 300 and 600 kHz to identify the backscatter textures of the seafloor and target the submerged archaeological artifacts. A stainless-steel fish was towed by a 5 m cable behind the survey vessel, the device emitted fan-shaped pulses towards the bottom and recorded a seafloor swath of 75 m range on each side. Five (NW-SE) track-lines parallel to the coast and the other two (NE-SW) perpendicular lines (Figure 2) were recorded by Edge-Tech (Discover) software in JSF format, while data processing was done through Geocoder and side scan mosaicking of Hypack® software. Initially, the SSS data underwent reformatting from JSF field format to HSX processing software format, then radiometric and geometric corrections were performed, auto Time Varying Gain amplifications were also applied to compensate for the decay in signal amplitudes, followed by slant range correction related to a reasonable sea bottom tracking. Then a final Geotiff mosaic image was constructed using the high frequency dataset (600 kHz), and the sonographs were classified according to the backscatter intensity.

Sub-bottom profiler survey (Figure 2) was carried out through three planned lines oriented (NW-SE) and four (NE-SW) cross lines by using chirp sub-bottom profiler (Edge-Tech 3200 series), the system comprised a transducer towed behind the survey vessel with 10 m cable-out applied subsequently in layback correction to position the tow-fish precisely, 20 ms acoustic impulse were emitted by the transducer with 100% pulse power and pinging (2–12 kHz) frequency range with a high rate to offers high resolution seismic records in the moderately shallow survey area, seismic data were recorded in JSF format using the native Discover software. Seismic data processing was applied using Hypack® sub-bottom software and the workflow included band-pass frequency filtering and time varying gains to produce a clear image for the stratigraphic interpretations. The seismic profiles were acquired in the time domain and horizon depths have been deduced using an average sound velocity of 1530 m/s acquired by (Valeport) sound velocity profiler. The identified horizons and their top surface ages have been tied with previously published sediment core samples (AL25 and AL19) around the study area (Figure 1c) which were obtained in ^{14}C radiocarbon years B.P. using the Accelerator Mass Spectrometry technique [5,7]. The core sample (AL25) lies inside the study area and was correlated with the core sample (AL19) which lies around 1 km to the east of the core sample (AL25). Subsequently, the lateral geomorphological variations were extrapolated across the subsurface profiles.

The ROV video camera dives and sediment grab sampling locations (Figure 2) were selected according to the preliminary interpretation of the acoustic data. Positioning and piloting of the ROV Video camera (Videoray pro3) were remotely done by the researchers from the survey vessel (Figure 3), where the control unit comprised a joystick and third axis controllers with a 15′ LCD screen which displays the video signal overlayed with the heading and depth readings. The position of the ROV video camera was estimated from the GPS NMEA output and the layback as a function of depth according to Vincentys algorithm [29].

Surface sediment samples were collected using a stainless-steel Peterson grab sampler, and locations were determined using DGPS. Grain size analyses were performed at the Marine Geophysics Lab of the National Institute of Oceanography and Fisheries, and the samples were subjected to the combined technique of pipette analysis and dry sieving [30]. Results of mean size and sorting of sediments were compared with the acquired seafloor images of the side scan sonar and the different backscattered forms were defined.

Figure 3. The researcher during the piloting of the ROV camera onboard the research vessel.

3. Results

3.1. Bathymetry

The resulted bathymetric contour map (Figure 4) has revealed the recent seafloor morphology of the study area. Generally, the depth values ranged from 1 m close to the coast to more than 10 m at the northeastern corner of the study area towards the center of the harbor. The 3.5 m contour line outlined a border for two opposite structures which are separated by relatively deeper area and interpreted as the two main breakwaters of the submerged ancient port that once settled above the seabed in this part of the harbor [1,31], the contour lines showed irregular patterns around these structures then increased regularly to 5 m towards the north, afterward the seafloor was sloped gently towards north till reaching 10 m depth. The contour shape of the shallower zone close to the coast (~less than 2 m depth) suggested the presence of a quay that was connected with the breakwaters of the submerged port.

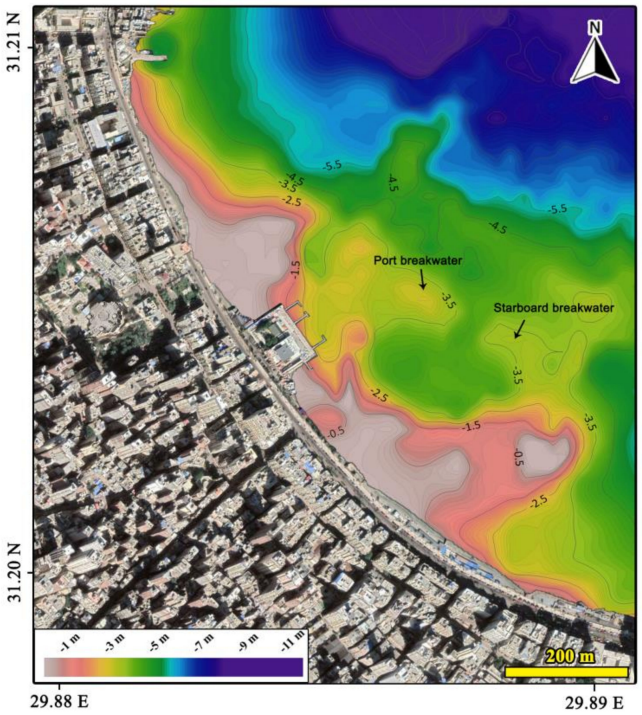

Figure 4. Bathymetric contour map of the study area showing the submerged ancient harbor.

3.2. Sonar Imaging

The mosaic map of the stacked side scan sonar images (Figure 5) defined the recent seafloor acoustic pattern of the study area according to variation in the backscatter intensity [22,25]. Generally, different forms of backscattered intensities were detected in the study area, the first form was characterized by a bright appearance due to the high backscatter intensity which defined the submerged archaeological remains, the outcropping reefs, and the coarse-grained sediments (Table 1). While the second form was encountered by a pale appearance as a result of the weak backscattered intensity which mainly indicated the presence of fine-grained sediments (Table 1), also some combined patches of bright and pale appearance were noticed in certain areas.

Figure 5. Side scan sonar mosaic map of the study area showing the traces of the submerged ancient harbor. (**a**) Very-coarse boulders; (**b**) Coarse boulders; (**c**) Buried archaeological remains; (**d**) Outcropping reefs.

Table 1. Results of mean size and sorting of sediments samples.

Sample Number	Sample Depth (m)	Sediment Type/ Mean Size	Sediment Sorting
1	3.3	Coarse sand	Poorly sorted
2	4.9	Fine sand	Moderately well sorted
3	3.4	Medium sand	Poorly sorted
4	4.1	Fine sand	Moderately sorted
5	4.3	Very Fine sand	Moderately sorted
6	3.2	Very Fine sand	Moderately well sorted

The mosaic map (Figure 5) showed semi-buried archaeological remains at 250 m away from the coastline, these remains are in the form of two asymmetric breakwaters of a submerged port structure, which spaced by 45 m from each other and this space was suggested to be the old port entrance. Target measurements were performed on the mosaic map and subsequently, the starboard-side breakwater of the submerged port was found extending for about 230 m with about 10 m widths that got thinned towards the entrance of the port, the height of this breakwater varied from 0.6 m from the seafloor up to 1.3 m at the western end. While the length of the 1 m elevated port-side breakwater was measured to be around 180 m and the width noticeably varied from 12 m at both ends and around 22 m at the central part. Other geomorphological changes have been noticed, where several groups of coarse and very-coarse boulders [32,33] were detected with distinct reflections around the eastern edge of the starboard breakwater (Figure 5a) and inside the port entrance (Figure 5b); in addition to traces of buried and deformed remains in the suggested quay area at the southwestern margin of the mosaic map (Figure 5c). Several outcropping reef

areas were recognized on the seafloor (Figure 5d) where a low relief area was located at 35 m offshore the breakwaters, another higher relief region was detected at 160 m apart from the breakwaters and elevated 1 m from the seafloor.

3.3. Ground-Truthing

The ROV camera dives generally gave cloudy images for the seafloor due to the high turbidity that provided less than 0.5 m forward visibility. Different features were captured (Figure 6) on the study area around the sampling locations, where outcropping reef area (Figure 6a), sand ripples (Figure 6b), breakwater remains (Figure 6c), scattered boulders (Figure 6d), soft sediments (Figure 6e), and irregular patches of sediments (Figure 6f) were recognized.

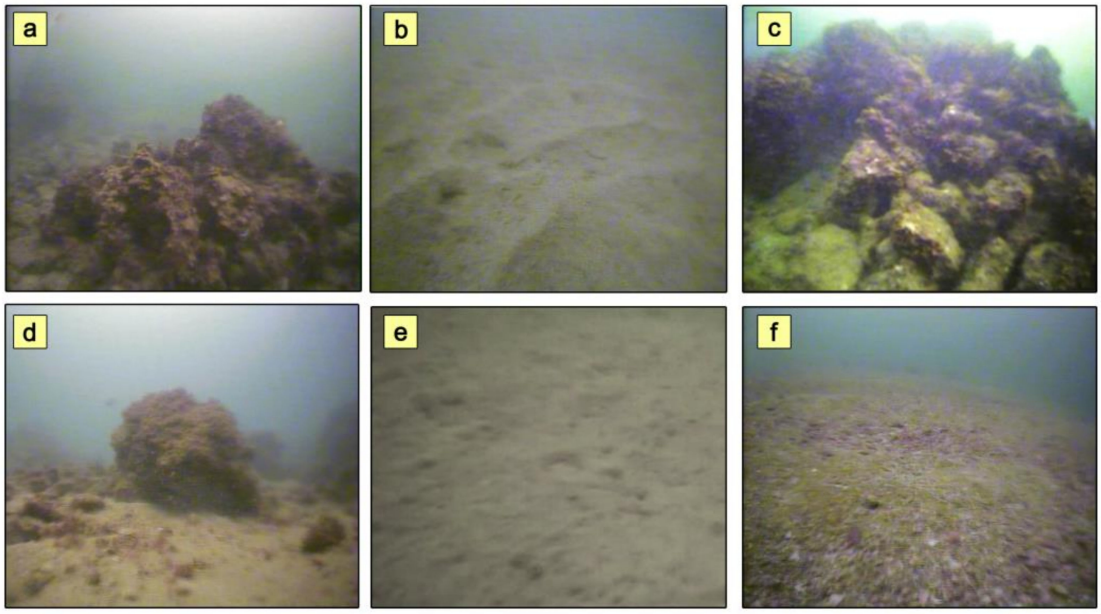

Figure 6. (**a**–**f**): Seafloor images obtained from the ROV camera dives around the six sampling stations (not to scale).

Results of sediments analyses (Table 1) were compared with the backscattered sonographs (Figure 5) and ROV dives images (Figure 6). Sediment types were classified on the mosaic map of the side scan sonar [25], where the poorly sorted coarse and medium-grained sands were represented by bright color tones on the sonographs, and appeared in the form of ripple marks which mainly located in high silting areas [34] especially around the submerged breakwaters and the outcropping reefs. While the dark color tones were represented by the moderately sorted fine-grained sediments that widely spread in the north-western and north-eastern parts of the study area. These dark tones were also located outside the port entrance, and around the borders of the port side breakwater.

3.4. Sub-Bottom Profiling

Interpretations of seismic profiles with the sediment core data [7] (Figure 7) showed the depositional sequence of the topmost sedimentary layers, and illustrated the evolution of seabed topography and bathymetric features, the suggested stratigraphic sequence was displayed through the seismic profiles [P] and [C] (Figure 2). Seismic profile [P] showed the borders of the two submerged breakwaters of the ancient port (Figure 8), these borders are marked by the top surface of the Ptolemaic era and tied with dated core samples [5,7], where the Royal ports of ancient Alexandria were developed during the Ptolemaic rule at Late Holocene epoch [9,14]. The port-side breakwater was found cutting through the sediments substrate and cropping out more than 3 m from the seabed, while the sediment thicknesses were varied across the sub-bottom profiles where it thickened up to 2 m in the area of the port entrance (Figure 8) and the area offshore the port-side breakwater

(Figure 9). The corresponding sedimentation of the Roman period is relatively low above the breakwater margins; also, the top surface of the Roman era was found onlapping over the port structures. Sharp reflections were noticed on the top surface of the Roman layer above the port structure and close to the port scarps (Figures 8 and 9). The sub-bottom profiles were found capped with a relatively thin layer of sediments corresponding to the later Arabic time till the present.

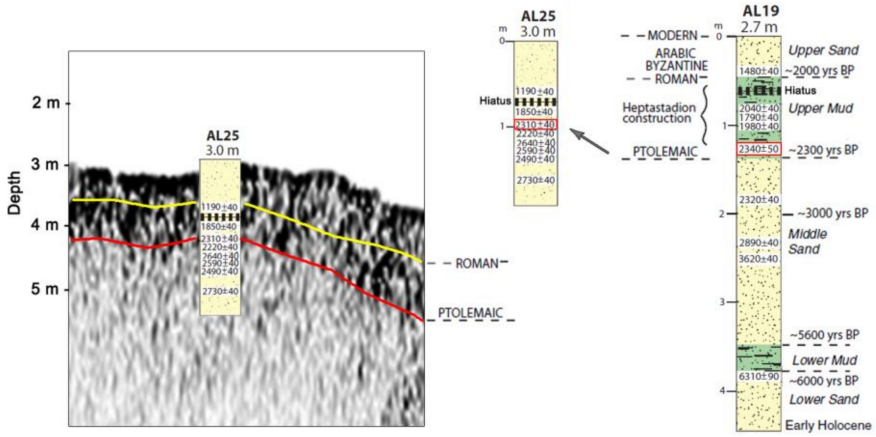

Figure 7. Core sample (AL25) tied with the SB profile (C) after correlation with core sample (AL19) (modified after Stanley et al., 2007 [7]).

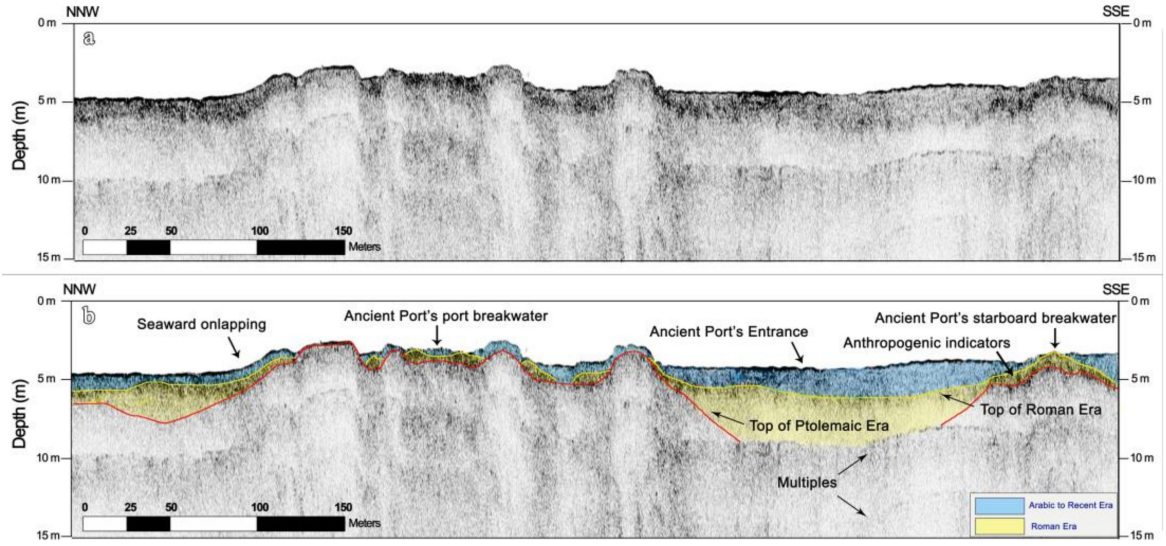

Figure 8. Seismic profile [P] across the breakwaters of the submerged ancient harbor. (**a**) Uninterpreted profile; (**b**) Interpreted profile.

Integration of Sonar images with sub-bottom profiles was applied to study each breakwater separately and to confirm the survey results, where the eastern part of the starboard-side breakwater was found outcropping and semi-buried in the sediment substrates and gradually get buried while moving towards the port entrance, the sediments were noticed onlapping over the western edge of the breakwater (Figure 10b), ripple marks were detected on the seabed around the outcropping region of the starboard-side breakwater, and several boulder debris were recognized spreading over different sediment patches around the port entrance (Figure 10a). The deformed surface of the port-side breakwater was noticed on the side scan sonar image (Figure 11a) where some parts were buried by sediments and others were outcropping, also the ancient sea scarp was noticed on the sonograph and indicated by onlapping sediments on the subsurface profile (Figure 11b).

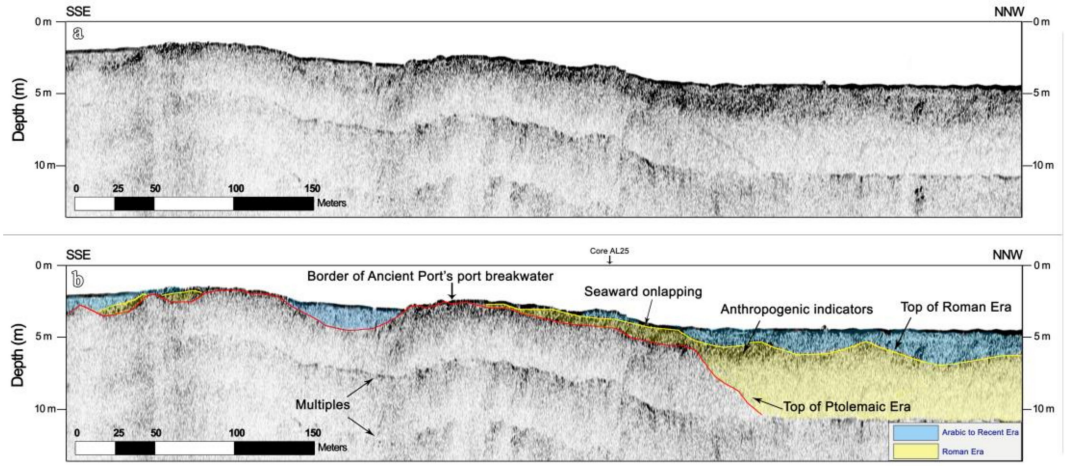

Figure 9. Seismic profile [C] across the Port side breakwater of the submerged ancient harbor. (**a**) Uninterpreted profile; (**b**) Interpreted profile.

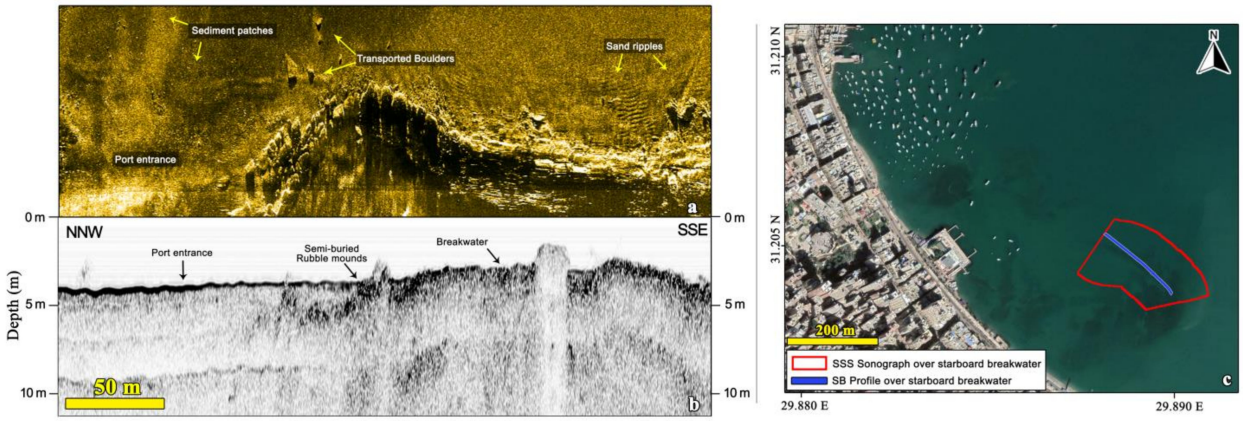

Figure 10. The starboard side breakwater of the submerged ancient harbor. (**a**) Side scan sonar image; (**b**) Sub-bottom profiler section; (**c**) Location map of the displayed images.

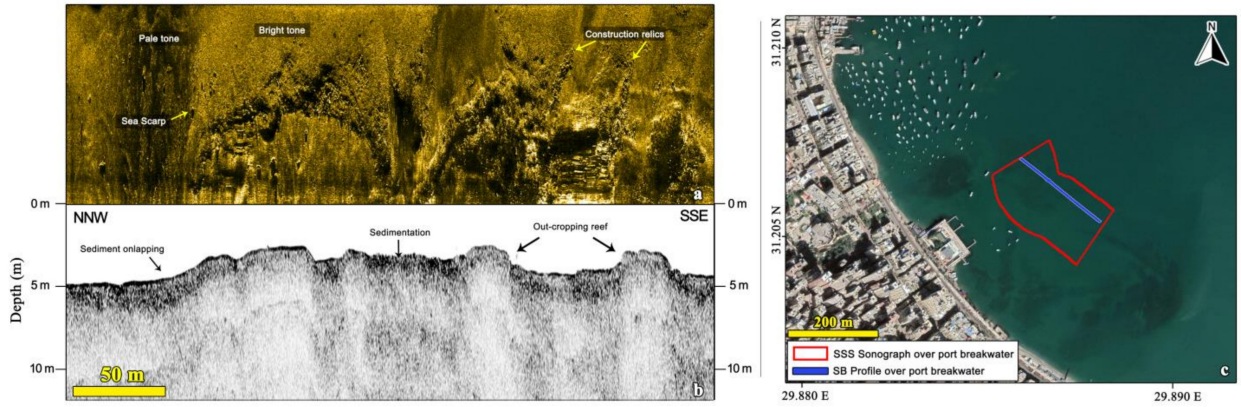

Figure 11. The port side breakwater of the submerged ancient harbor. (**a**) Side scan sonar image; (**b**) Sub-bottom profiler section; (**c**) Location map of the displayed images.

3.5. Sediment Thickness

The sediment thickness was interpolated for the successive sedimentary layers presented in the sub-bottom profiles across the study area, where the lower succession represents the sedimentation during the Roman period (Figure 12), while the upper layer represents the Arabic to Recent period (Figure 13). The sediment thickness of the Roman

period has a range of 0.1–3 m, a maximum thickness of 3.2 m was observed in the western and north-eastern parts, and a minimum thickness of 0.2 m was noticed in the southern and eastern margins. Generally, the thickness of the lower layer varies according to the seabed topography, which reaches around zero where the outcropping rocks and submerged structures exist.

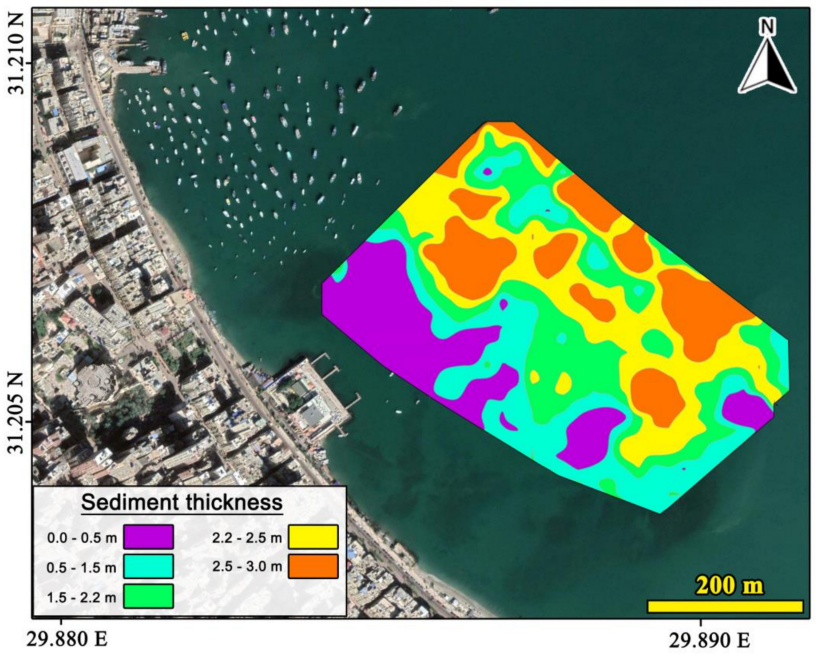

Figure 12. Isopach map for the sedimentation during the Roman period in the study area.

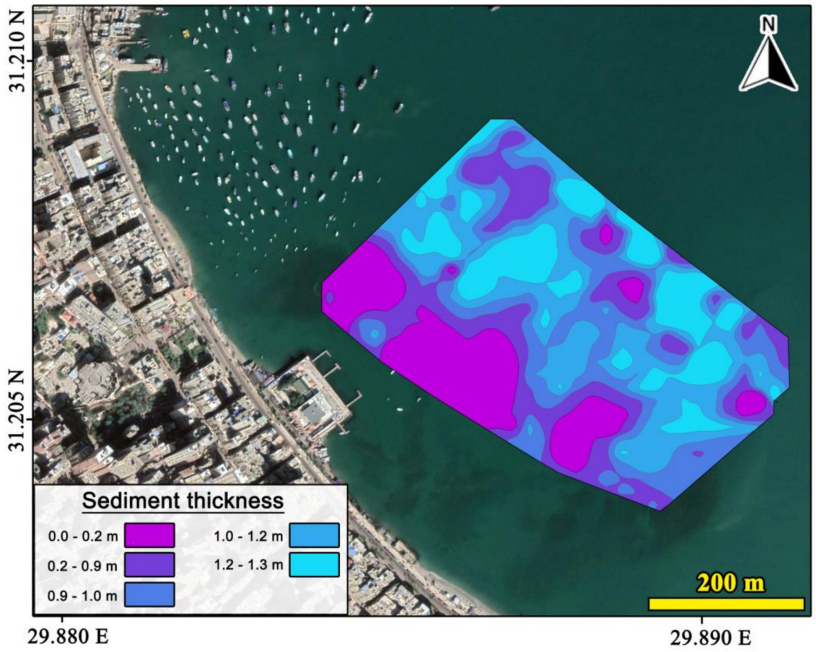

Figure 13. Isopach map for the sedimentation during the Arabic to Recent period in the study area.

The sediment thickness of the upper succession corresponding to the Arabic to Recent period (Figure 13) has a range of 0.1–1.3 m, the sediment is much thicker in the northeastern part reaching 1.5 m, and much thinner in the southern parts close to the shore, that reach around zero at the outcropping rocks and the submerged structures.

4. Discussion

The ancient coast of Alexandria was significantly modified during the Greek and Roman periods after the destruction of the royal ports and palaces as a result of land subsidence, eustatic sea-level rise, earthquakes, and tsunami. Mapping of the submerged ancient site which was constructed during the Ptolemaic period in the 4th century B.C. [9,35] allowed to detect remarkable geomorphological changes over the seabed of the study area across the past times.

The bathymetric mapping and the sonar imaging for the seafloor topography and the seabed characteristics have defined the supposed borders of the submerged port site, the noticed asymmetry in the shape of both breakwaters indicated mostly that the starboard-side breakwater was artificially built over the seafloor due to the presence of a large number of rubble mounds along this breakwater (Figure 10a), while the rough surface of the port-side breakwater indicated that the breakwater was a part of a pre-existed out-cropping reefs; also, some construction relics were situated close to the reef structure of the breakwater (Figure 11a).

The non-uniform surfaces of breakwaters and the surrounding debris of coarse boulders were suggested to be an impact of the previously-recorded high magnitude natural hazards that affected the area. It is assumed that numerous fractions were disintegrated from the breakwaters forming debris of boulders, and transported away from the port structure, where storms and tsunami waves can hit and damage the ancient structures [36] and displace large boulders [37] due to its powerful carving abilities. The detected buried structures of the suggested quay of the port in the southwestern part of the study area have indicated the exposure of the port to a high silting rate due to the relatively rapid submergence as a result of the pre-mentioned catastrophic events. The majority of these geomorphological features were matched with the resulted images from the ROV camera dives. Also, seabed sediments were acoustically classified according to variation in the magnitude of backscatter intensity, the classification was calibrated by the results of grain size analyses of sediment samples, and specified that the fine-grained sediments represent darker color tones on the sonographs than the coarse-grained sediments.

The sub-bottom profiling survey showed the borders of the submerged breakwaters of the ancient port where the artificial rubble mounds of the starboard-side breakwater were noticed on the subsurface profile as an anomalous formation that buried within sedimentations and inclined towards the port entrance (Figure 10b), while the reef structure of the port-side breakwater was recognized as a base layer underneath the sediment layer (Figure 11b); also, the sedimentation onlapped over the breakwater seaward margin which marking a shore scarp. Several sharp reflections were noticed on the top surface of the Roman layer in the form of dark patches (Figure 8, Figure 9) which may indicate the presence of disturbed subsurface layers due to the incompetent anthropogenic activities related to the construction piling throughout the Roman period, during Alexandria's expansion [7,19,38], which acted as an indirect factor in the submergence of the archaeological site.

The variation in sediment thicknesses along the port margins has indicated changing sedimentation rates across the past times (Figures 12 and 13), where the sediment thickness between the opposite breakwaters is larger than the thickness across the breakwater margins, this condition was suggested to be a result of the increased rates of depositions that followed the construction of the Heptastadium tombolo which changed the current circulations and sediment deposition around the port structure through the late Ptolemaic era [7], also due to the high silting accompanied with the 365 A.D tsunami waves during the Roman period [35,39] which in turn buried the structures of the ancient port and the port entrance space by sediments alluviations, from the isopach maps, it is clear that the sediment accumulations during the Roman period (Figure 12) were larger than that of the Arabic to Recent period (Figure 13). Also, the determined thicknesses perfectly matched with the historical records of ~2 m sea-level rise and land subsidence during the last two millennia [14].

Integration of the acoustic data with the results of sediment analyses and ROV images provided a clear image for the recent seabed characteristics by establishing a synthetic classification map (Figure 14). Different forms of features were recognized on the seabed, where the fine-grained sediments covered the majority of the study area, while the medium to coarse-grained sediments spread in the central part and bounded the submerged structure of the ancient port. The submerged structure was surrounded by different-sized disintegrated boulders that scattered towards the southern shore next to various partially buried remains. Also, outcropping reef and rocky areas were located in the central part and the south-eastern margin of the study area, respectively.

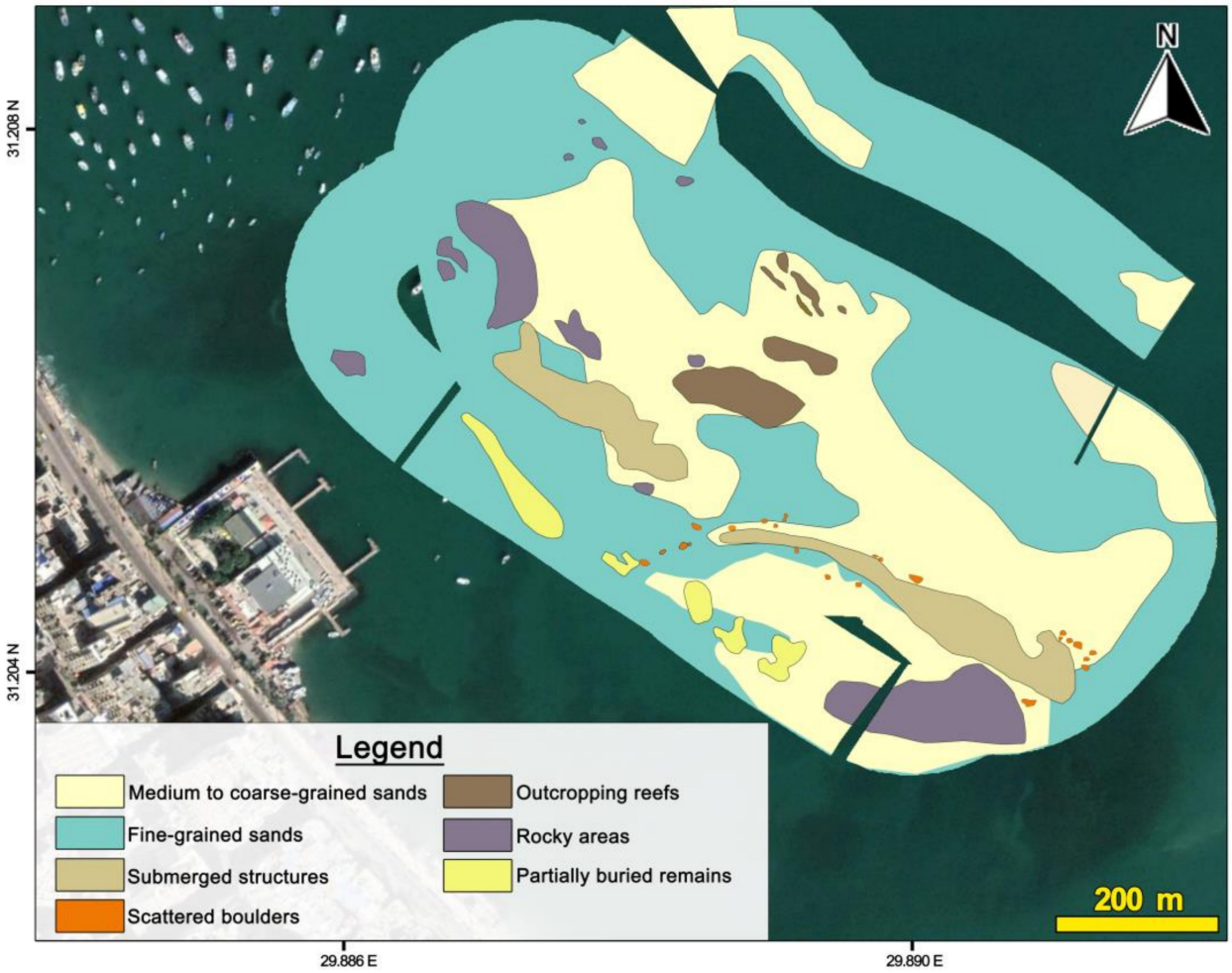

Figure 14. Synthetic classification map resulted from combining the mosaic image with the sediment classification results.

5. Conclusions

The geophysical mapping of the submerged archaeological site showed significant results in seabed investigation and detection of the possible geomorphological changes resulted from the sea-level rise and natural hazards. The acoustic data were integrated with the acquired surface samples and the previously dated sedimentological core data, in addition to records of relative sea-level rise.

The bathymetric mapping has revealed the recent sea-floor morphology outlining two breakwaters corresponding to a submerged ancient port, and the contour shape showed irregular patterns around the port structures and suggested the presence of a quay in the shallow coastal zone of the study area. While the sonar imaging survey has defined two different forms of backscattered intensities according to variation in the magnitude of the reflected energy. Partially buried archaeological remains were recognized

and interpreted as submerged breakwaters of an ancient port; also, coarse and very coarse boulders were detected around the submerged breakwaters in the form of debris that disintegrated from the submerged structure. The irregular structural form and the non-uniform surfaces of the submerged breakwaters highlighted the effect of severe natural hazards on the study area. Sediment types were classified on the mosaic map and ground-truthed with surface sediment samples and ROV camera images establishing a synthetic classification map that shows sediment and backscatter intensity distributions across the study area, where patches of sand ripples and relatively fine-grained sediments were distributed around the outcropping structures.

Interpretation of sub-bottom profiles has suggested the stratigraphic sequence of the topmost sedimentary layers and detected the borders of the submerged breakwaters of the ancient port, which indicated that each side had a different origin. Seaward sediment onlapping was noticed along the margin of the port structure which indicated the ancient shore scarps. The deposited sediment thicknesses varied across the subsurface profiles which increased in certain areas as a result of the changed current circulations following the construction of the Heptastadium tombolo and also due to the 365 A.D. catastrophic tsunami. Also, several indicators of anthropogenic activities were noticed on top of the Roman layer and capped with relatively thin deposition corresponding to the Arabic to the recent period. The results of these integrated geophysical techniques outlined the role of natural hazards and sea-level rise in changing the geomorphology of the coastline and seabed features.

Author Contributions: Conceptualization, A.H., N.E.-G., A.E.-S., S.E.-G. and A.F.; methodology, S.E.-G. and A.F.; software, A.F.; data acquisition, S.E.-G. and A.F.; writing—original draft preparation, A.H., S.E.-G. and A.F.; writing—review and editing, A.H., N.E.-G. and A.E.-S.; visualization, A.F.; supervision, A.H., N.E.-G. and A.E.-S. All authors have read and agreed to the published version of the manuscript.

Funding: This research received no external funding.

Data Availability Statement: The data presented in this study are owned by the National Institute of Oceanography and Fisheries and can be available on request.

Acknowledgments: The authors would like to express their gratitude to Marine Geophysics Lab members, "Mahmoud Salah" and "Mohamed Nassar" for their assistance in data acquisition. We also would like to thank Quaternary editors for their assistance and the two anonymous reviewers whose comments definitely improved the paper.

Conflicts of Interest: The authors declare no conflict of interest.

References

1. Goddio, F.; Bernand, A.; Bernand, E.; Darwish, I.; Kiss, Z.; Yoyotte, J. *Alexandria: The Submerged Royal Quarters*; Periplus: London, UK, 1998; p. 274.
2. Belov, A. Navigational Aspects of Calling to the Great Harbour of Alexandria. 2014; Halshs-00845524. Available online: https://halshs.archives-ouvertes.fr/halshs-00845524/file/Belov.A._forthcoming_Navigational_aspects_of_calling_to_the_Great_Harbour_of_Alexandria.pdf (accessed on 1 July 2021).
3. Mahmoud-Bey, M. *Mémoire sur l'Antique Alexandrie*; Imprimerie de Bianco Luno: Copenhagen, Denmark, 1872; p. 132.
4. Schwartz, S. *A Preliminary Survey of the Eastern Harbor, Alexandria, Egypt Indicating a Comparison of Side Scan Sonar and Remote Viewing*; Massachusetts Institute of Technology: Cambridge, MA, USA, 1980.
5. Stanley, J.D.; Bernasconi, M. Holocene Depositional Patterns and Evolution in Alexandria's Eastern Harbor, Egypt. *J. Coast. Res.* **2006**, *22*, 283–297. [CrossRef]
6. Torab, M. Paleo-geomorphological map of Alexandria site, Egypt by using submerged archaeological and other evidences. In *International Conference on Agriculture, Science and Engineering (ICASE2013)*; Federal College of Education: Umunze, Nigeria, 2013.
7. Stanley, J.D.; Carlson, R.; Beek, G.; Jorstad, T.; Landau, E. Alexandria, Egypt, before Alexander the Great: A multidisciplinary approach yields rich discoveries. *GSA Today* **2007**, *17*, 4–10. [CrossRef]
8. AbdelNaby, H. Problems and Challenges of Cultural Heritage in Alexandria, Egypt. *Int. J. Cult. Hist.* **2017**, *3*, 174–178. [CrossRef]
9. Jondet, M.G. *Les Ports Submergés de l'Ancienne île de Pharos*; Mémoires de l'Institut d'Egypte: Cairo, Egypt, 1916; p. 101.
10. Chen, Z.; Warne, A.G.; Stanley, J.D. Late quaternary evolution of the northwestern Nile Delta between the Rosetta promontory and Alexandria, Egypt. *J. Coast. Res.* **1992**, *8*, 527–561.

11. Guidoboni, E.; Comastri, A.; Traina, G. *Catalogue of Ancient Earthquakes in the Mediterranean Area up to the 10th Century*; Instituto Nazionale di Geofisica: Bologna, Italy, 1994; p. 504.
12. Stanley, J.D.; Bernhardt, C.E. Alexandria's eastern harbour, Egypt: Pollen, microscopic charcoal, and the transition from natural to human-modified basin. *J. Coast. Res.* **2010**, *26*, 67–79. [CrossRef]
13. Lambeck, K.; Esat, T.M.; Potter, E.-K. Links between climate and sea levels for the past three million years. *Nature* **2002**, *419*, 199–206. [CrossRef]
14. Stanley, J.-D.; Landau, E.A. Early human activity (pre-332 BC) in Alexandria, Egypt: New findings in Eastern Harbor cores, Eos. Transactions. *Am. Geophys. Union Fall Meet. Suppl.* **2005**, *86*, F1252.
15. Mitrovica, J.; Milne, G. On the origin of late Holocene sea-level highstands within equatorial ocean basins. *Quat. Sci. Rev.* **2002**, *21*, 2179–2190. [CrossRef]
16. Pirazzoli, P.; Laborel, J.; Stiros, S. Earthquake clustering in the Eastern Mediterranean during historical times. *J. Geophys. Res.* **1996**, *101*, 6083–6097. [CrossRef]
17. Kebeasy, R. Seismicity. In *The Geology of Egypt*; Said, R., Ed.; A.A. Balkema: Rotterdam, The Netherlands, 1990; pp. 51–59.
18. Malaval, B.; Jondet, G. *Le Port d'Alexandrie. Cairo: Administration des Ports et Phares*; Imprimerie Nationale: Paris, France, 1912; p. 84.
19. Stanley, J.-D.; Jorstad, T.F.; Goddio, F. Human impact on sediment mass movement and submergence of ancient sites in the two harbours of Alexandria, Egypt. *Nor. J. Geol.* **2006**, *86*, 337–350.
20. El-Asmar, H.; Ahmed, M.; Taha, M.; Assal, E.M. Human Impacts on Geological and Cultural Heritage in the Coastal Zone West of Alexandria to Al-Alamein, Egypt. *Geoheritage* **2012**, *4*, 263–274. [CrossRef]
21. Westley, K.; Quinn, R.; Forsythe, W.; Plets, R.; Bell, T.; Benetti, S.; McGrath, F.; Robinson, R. Mapping submerged landscapes using multibeam bathymetric data: A case study from the north coast of Ireland. *Int. J. Naut. Archaeol.* **2011**, *40*, 99–112. [CrossRef]
22. Hamouda, A.Z.; EL-Gendy, N.; El-Gharabawy, S.; Salah, M. Acoustic Survey along Heraklieon and East Canopus Ancient Greek Cities, Abu Quir Bay, Alexandria, Egypt. *J. Earth Sci. Clim. Chang.* **2015**, *6*, 289.
23. Quinn, R.; Forsythe, W.; Breen, C.; Boland, D.; Lane, P.; Omar, A.L. Process-based models for port evolution and wreck site formation at Mombasa, Kenya. *J. Archaeol. Sci.* **2007**, *34*, 1449–1460. [CrossRef]
24. Chalari, A.; Papatheodorou, G.; Geraga, M.; Christodoulou, D.; Ferentinos, G. A marine geophysical survey illustrates Alexandria's Hellenistic past. *Zeitschrift Geomorphologie* **2009**, *53*, 191–212. [CrossRef]
25. Hamouda, A.Z.; EL-Gendy, N.; El-Gharabawy, S.; Fekry, A. Geological implications of acoustic imagery of the recent seabed textures in the Eastern Harbor, Alexandria. *EJAR* **2016**, *42*, 249–259. [CrossRef]
26. Papatheodorou, G.; Geraga, M.; Ferentinos, G. The Navarino naval battle site, Greece–an integrated remote sensing survey and a rational management approach. *Int. J. Naut. Archaeol.* **2005**, *34*, 95–109. [CrossRef]
27. Lee, G.H.; Kim, H.J.; Kim, D.C.; Yi, B.Y.; Nam, S.M.; Khim, B.K.; Lim, M.S. The acoustic diversity of the seabed based on the similarity index computed from Chirp seismic data. *ICES J. Mar. Sci.* **2009**, *66*, 227–236. [CrossRef]
28. Geraga, M.; Papatheodorou, G.; Agouridis, C.; Kaberi, H.; Iatrou, M.; Christodoulou, D.; Fakiris, E.; Prevenios, M.; Kordella, S.; Ferentinos, G. Palaeoenvironmental implications of a marine geoarchaeological survey conducted in the SW Argosaronic gulf, Greece. *J. Archaeol. Sci. Rep.* **2017**, *12*, 805–818. [CrossRef]
29. Vincenty, T. Direct and inverse solutions of geodesics on the ellipsoid with application of nested equations. *Surv. Rev.* **1975**, *23*, 88–93. [CrossRef]
30. Folk, R.L. *Petrology of Sedimentary Rocks*; Hemphill Publishing Company: Austin, TX, USA, 1974.
31. Fraser, P.M. *Ptolemaic Alexandria*; Oxford University Press: London, UK, 1972; p. 2136.
32. Ruban, D.A.; Sallam, E.S.; Ermolaev, V.A.; Yashalova, N.N. Aesthetic Value of Colluvial Blocks in Geosite-Based Tourist Destinations: Evidence from SW Russia. *Geosciences* **2020**, *10*, 51. [CrossRef]
33. Terry, J.; Goff, J. Megaclasts: Proposed Revised Nomenclature At the Coarse End of the Udden-Wentworth Grain-Size Scale for Sedimentary Particles. *J. Sediment. Res.* **2014**, *84*, 192–197. [CrossRef]
34. Hamouda, A.Z.; El-Gharabawy, S.; Fekry, A.; Nassar, M.; Salah, M. Subsidence model of the ancient Alexandria Royal port linked to sea-level rise and natural hazards using integrated geophysical methods. *EJAR* **2021**, in press.
35. Goiran, J. Recherche Géomorphologique dans la Région Littorale d'Alexandrie, Egypte: Mobilité des Paysages à l'Holocène Récent et Évolutiondes Milieux Portuaires Antiques. Ph.D. Thesis, Université d'AixMarseille, I-Cerege, Marseille, France, 2001.
36. Reinhardt, E.; Goodman-Tchernov, B.; Boyce, J.; Van, P.; Rink, W.J.; Mart, Y.; Raban, A.; López, G. The tsunami of 13 December A.D. 115 and the destruction of Herod the Great's harbor at Caesarea Maritima, Israel. *Geology* **2006**, *34*, 1061–1064. [CrossRef]
37. Torab, M.; Dalal, N. Natural hazards mapping of mega waves on the NW coast of Egypt. *J. Afr. Earth Sci.* **2015**, *112*, 353–357. [CrossRef]
38. Véron, A.; Goiran, J.P.; Morhange, C.; Marriner, N.; Empereur, J.Y. Pollutant lead reveals the pre-Hellenistic occupation and ancient growth of Alexandria, Egypt. *Geophys. Res. Lett.* **2006**, *33*, L06409. [CrossRef]
39. Hamouda, A.Z. A reanalysis of the AD 365 tsunami impact along the Egyptian Mediterranean coast. *Acta Geophys.* **2010**, *58*, 687–704. [CrossRef]